
Article:
Dedrick, James Peter orcid.org/0000-0003-4353-104X, Gibson, Andrew Robert orcid.org/0000-0002-1082-4359, Rafalskyi, Dmytro et al. (1 more author) (2017) Transient propagation dynamics of flowing plasmas accelerated by radio-frequency electric fields. Physics of Plasmas. pp. 1-5. ISSN 1089-7674

https://doi.org/10.1063/1.4983059

Transient propagation dynamics of flowing plasmas accelerated by radio-frequency electric fields

James Dedrick

York Plasma Institute, University of York, YO10 5DD York, UK

Andrew Robert Gibson

York Plasma Institute, University of York, YO10 5DD York, UK and

LPP-CNRS, Ecole Polytechnique, route de Saclay, 91120 Palaiseau, France

Dmytro Rafalskyi and Ane Aanesland

LPP-CNRS, Ecole Polytechnique, route de Saclay, 91120 Palaiseau, France

Flowing plasmas are of significant interest due to their role in astrophysical phenomena and potential applications in magnetic-confined fusion and spacecraft propulsion. The acceleration of a charge-neutral plasma beam using the radio-frequency self-bias concept could be particularly useful for the development of neutralizer-free propulsion sources. However, the mechanisms that lead to space-charge compensation of the exhaust beam are unclear. Here, we spatially and temporally resolve the propagation of electrons in an accelerated plasma beam that is generated using the self-bias concept with phase-resolved optical emission spectroscopy. When combined with measurements of the extraction-grid voltage, ion and electron currents, and plasma potential, the pulsed-periodic propagation of electrons during the interval of sheath collapse at the grids is found to enable the compensation of space charge.

The interesting fundamental physics of plasma acceleration [1–3], and its potential applications in thermonuclear fusion [4, 5] and spacecraft propulsion [6–8] have driven significant research interest. Gridded-ion and Hall-effect thrusters are now established propulsion technologies [9], and plasma thrusters that can operate without an external neutralizer are under development [10, 11].

Using the *Neptune* plasma-thruster prototype, the acceleration of a broad, collimated and charge-neutral plasma beam, without the use of an external neutralizer, has recently been demonstrated to exhibit comparable performance to traditional gridded-ion propulsion sources [12, 13]. Its design is based around the principle of plasma acceleration, whereby the coincident extraction of ions and electrons is achieved by applying an oscillating electrical field to the gridded acceleration optics. In traditional gridded-ion thrusters, ions are accelerated using a designated voltage source to apply a direct-current (dc) electric field between the extraction grids. In this work, a dc self-bias voltage is formed when radio-frequency (rf) power is coupled to the extraction grids due to the difference in area of the powered and grounded surfaces in contact with the plasma.

To maximise thrust efficiency using a single rf power source, it is important to regulate the electron and ion fluxes that vary on nanosecond time scales. Further, boundary conditions in the plasma source and diffusion region can play a significant role in determining the plasma propagation behaviour [14]. These require a more detailed understanding of the beam dynamics with respect to distance, time and particle energy.

Non-invasive optical diagnostic techniques have previously proven useful to the investigation of electric propulsion sources, providing enhanced spatial resolution compared to electrostatic probes. For example, optical emission spectroscopy has been used to measure neutral-gas heating in electrothermal plasma thrusters [15], and imaging and laser induced fluorescence velocimetry are effective for the study of cross-field electron transport [16] and ion velocities [17] in Hall-effect thrusters.

Of particular importance to space-charge compensation in the *Neptune* beam are the spatially and temporally resolved electron dynamics at the extraction grids. Phase-resolved optical emission spectroscopy (PROES), which enables the spatial and temporal dynamics of selected excited species to be measured on nanosecond time scales [18, 19], has successfully been applied to low-pressure [20–25] and atmospheric-pressure [26–28] capacitively coupled plasmas. Here, we use PROES to directly observe the transient propagation of energetic

electrons to determine their role in compensating space charge in the exhaust beam.

The experimental setup is shown in Figure 1. *Neptune* comprises an inductively coupled plasma source (ICP: Teflon-insulated $8 \times 12 \times 12$ cm^3 cavity, ferrite-enhanced 7-turn planar antenna driven at 4 MHz, 2 mm thick ceramic window) operated in H-mode and two rectangular extraction grids (stainless steel, optical transparency 0.6, aperture diameter 2.5 mm, inter-grid distance 2 mm) that are used to accelerate ions.

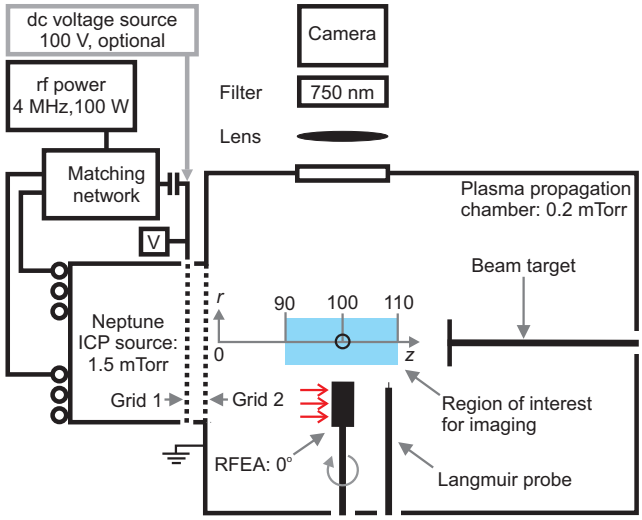

FIG. 1. Illustration of the experimental setup. For electrical measurements the beam target, Langmuir probe and retarding field energy analyser (RFEA) can be positioned at $(r, z) = (0, 100)$ mm as shown by the open circle, and these are removed for measurements of the optical emission with the camera. The RFEA can be rotated to face the plasma source (rotation angle 0° shown) or in the r-direction (rotation angle 90°). During 'rf operation', rf power is distributed between the ICP coil and extraction grids. In 'dc operation', rf power is coupled to the ICP coil only and a dc voltage source is connected across the grids.

During 'rf operation', rf power at 100 W is distributed between the ICP coil and Grid 1 (closest to the cavity as shown in Figure 1) using an impedance matching network and blocking capacitor, while Grid 2 is electrically grounded. These conditions correspond to a time-varying, approximately sinusoidal voltage waveform at the extraction grids with a peak-to-peak voltage $V = 200$ V and a time-averaged self-bias voltage $V_{\rm sb} = 100$ V (see Figure 4 (a) later). During 'dc operation' (described further below) rf power is coupled to the ICP coil only and a 100 V dc voltage source is connected across the extraction grids.

Neptune is connected to a plasma-propagation chamber (1 m long, 0.7 m diameter,

2500 L/s pumping rate) and is fed with 25 sccm of argon. Under these conditions the source pressure is 1.5 mTorr, while that in the propagation chamber is 0.2 mTorr.

An intensified charge coupled device camera (ICCD: *Andor iStar* 320T, 1024 $\times$ 256 pixel array, 26 μm^2 pixel area) is used to detect the optical emission from the plasma beam through a view port in the propagation chamber. This enables a 20×7.5 mm^2 region-of interest that is axially elongated and centred at $z = 100$ mm as shown in Figure 1. The spatial resolution of the optical measurements is determined to be 26.7 pixel/mm. Measurements are undertaken using a 50 ns gate width and a 50 ns gate step. Images are acquired with a sampling frequency of 500 kHz for an exposure time of 20 s. The observed optical emission is therefore integrated over thousands of rf cycles to ensure reproducibility.

The ICCD is fitted with an interference filter for spectral discrimination. This has a central wavelength 750 nm and full width at half maximum of 10 nm, and hence the transitions under consideration are Ar($2p_1 - 1s_2$) at 750.4 nm and Ar($2p_5 - 1s_4$) at 751.5 nm. Cascade processes from higher-energy excited states into the Ar($2p_1$) level are understood to have only a minor influence under these conditions, but could play a more significant role for the Ar($2p_5$) level [29]. In the absence of cascade processes, the measured optical emission is considered to be indicative of electrons with energy greater than 13.48 eV for direct-impact excitation of the Ar($2p_1$) level. However, since we cannot exclude the optical emission at 751.5 nm from the Ar($2p_5$) level, the contribution from cascade processes cannot be neglected. If significant, this would result in an increase in the effective lifetime of the optical emission and a decrease in the temporal variations observed.

For electrical measurements, a Langmuir probe (LP), rf-compensated retarding field energy analyser (RFEA), and floating beam target are positioned in the centre of the region-of-interest at $(r, z) = (0, 100)$ mm as shown in Figure 1. These enable measurements of the on-axis and isotropic electron energy probability functions (EEPFs), on-axis ion energy distribution function (IEDF), together with the electron current, ion current and beam potential with respect to time. For EEPF measurements, the LP is used to detect (isotropic) electrons of energy $0 < E_e < 12$ eV, and the RFEA can be rotated such that it faces the source along the z-axis (0° rotation angle) or in the perpendicular r-direction (90° rotation angle) for collection of directed and isotropic electron fluxes, respectively, of energy $12 < E_e < 21$ eV.

As shown in Figure 2 (a), during rf operation a multi-peaked and broad IEDF is ob-

served, which is consistent with the similar values of the 4 MHz grid voltage and ion-plasma frequencies [30]. It is also in agreement with previous measurements, where multiple peaks in the spectrum were suggested to be caused by a spatially varying sheath profile at the multi-aperture extraction grids [12].

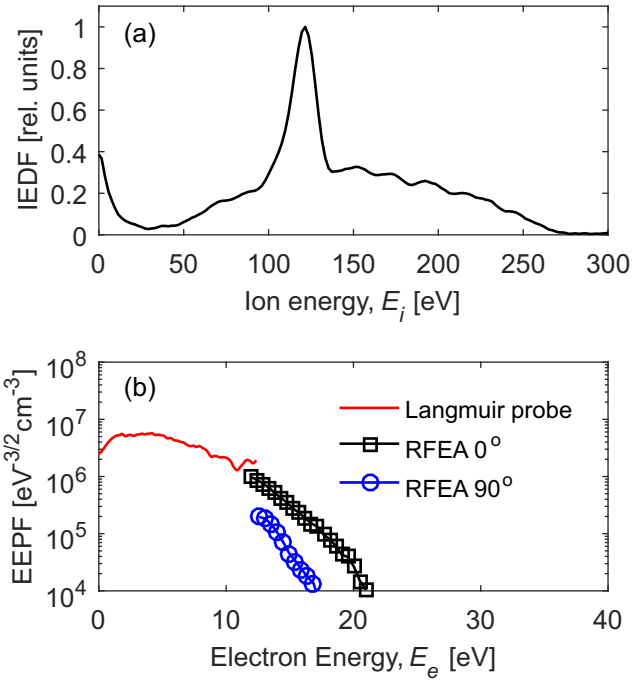

FIG. 2. (a) Ion energy distribution function (IEDF) and (b) electron energy probability functions (EEPFs) measured with a Langmuir probe over 0-12 eV and 12-21 eV using a rotating retarding field energy analyser (RFEA) during rf operation.

Measurements of the EEPF, shown in Figure 2 (b) for isotropic (LP, RFEA 90°) and on-axis (RFEA 0°) orientations, demonstrate the presence of an anisotropic electron beam. These electrons could be accelerated by a local reversal of the electric field during the Grid 1 sheath collapse [31]. As the electron beam is propagating in the same direction as the ion flux the conditions are consistent with the presence of an accelerated plasma beam [13].

To investigate the electron dynamics with reference to traditional dc gridded-ion sources, the thruster is operated in two modes as described above: 'rf operation' where rf power is distributed between the ICP and extraction grids resulting in a dc self-bias voltage $V_{\rm sb} = 100$ V, and 'dc operation' where a dc bias voltage $V_{\rm dc} = 100$ V is applied across the extraction grids and the ICP is driven by the rf power source. For simplicity, no cathode neutralizer is used

in the study of dc operation. Beam stalling is avoided due to its self-compensation in the grounded propagation chamber, together with a relatively high gas pressure greater than 0.1 mTorr [32]. Here, the transport conditions have been continuously controlled using measurements of the beam potential at the source exit and the ion flux. The power dissipated in the extraction grids is comparable between rf and dc operation [13].

Figure 3 (a) and (b) show the variation in optical emission with respect to time and axial distance (radially averaged) for rf and dc operation, respectively. In rf operation, electrons with energy greater than 13.48 eV are observed to propagate axially from the source once per 250 ns rf cycle, as observed through a 20 % increase in the optical-emission intensity for intervals commencing at 50 ns, 300 ns, and 550 ns. The relatively weak temporal modulation observed in rf operation is indicative of cascade contributions to the excitation of the $\mathrm{Ar}(2p_5)$ level as discussed earlier.

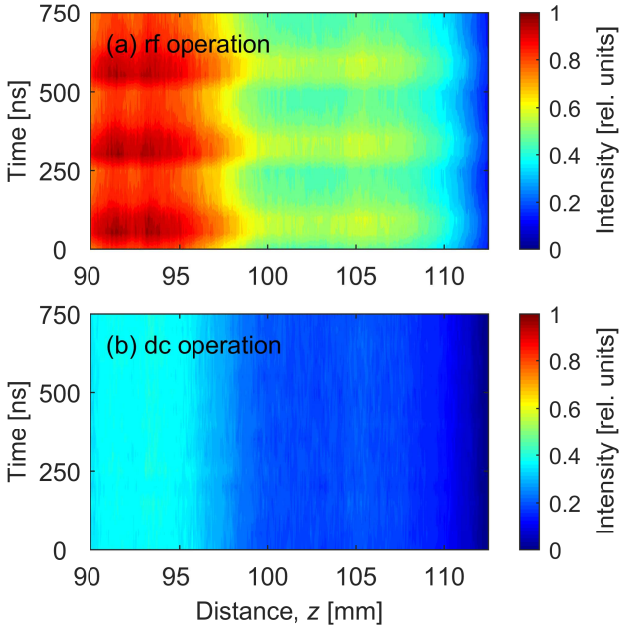

FIG. 3. Intensity of the optical emission with respect to axial distance for (a) rf operation and (b) dc operation.

Together with the periodic optical-emission structures that are evident across the region-of-interest, over $90 < z < 97$ mm the intensity is observed to drop by approximately 50 % as shown in Figure 3 (a). Similar behaviour is evident during dc operation, shown in Figure 3 (b), for which no temporal modulation in the optical emission is observed.

It is important to note that the maximum intensity of the optical emission observed during

dc operation is significantly lower (approximately 40 %) than for rf operation because the dc electric field applied across the extraction grids acts to confine electrons in the source region.

The role of pulsed-periodic electron fluxes on space-charge compensation during rf operation is studied by comparing the voltage at the extraction grids, spatially averaged and time-resolved optical emission, ion current, electron current, and beam potential. As shown in Figure 4 (a), the voltage applied across the extraction grids reaches $V = 0$ V once per rf cycle. This corresponds to the sheath collapse at Grid 1 and the propagation of electrons in the positive z-direction.

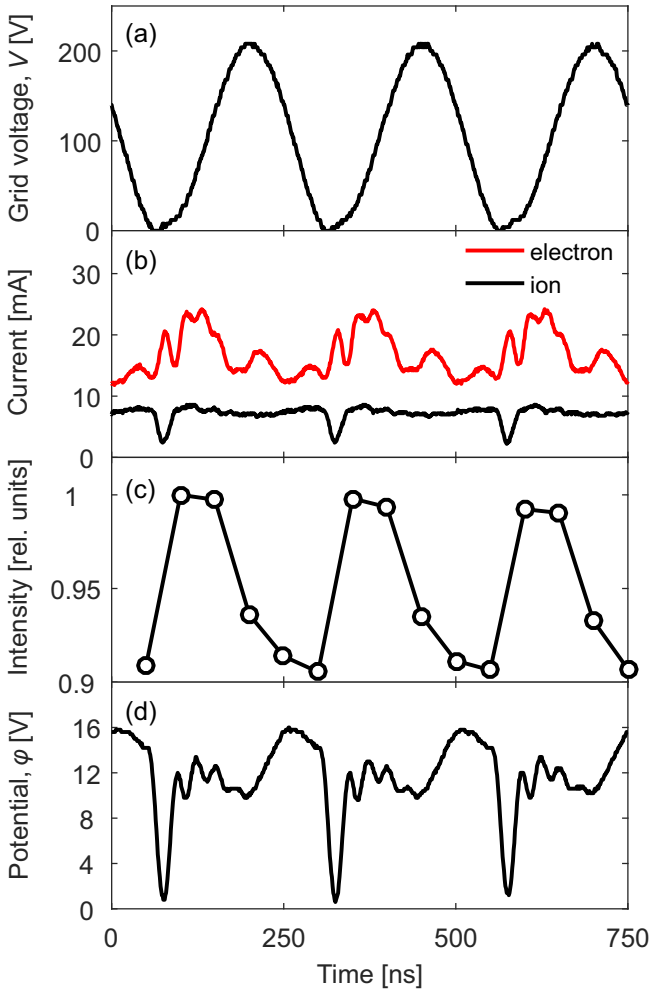

FIG. 4. (a) Voltage applied to the extraction grids and the (b) electron and ion currents, (c) spatially averaged optical emission (solid lines added for clarity), and (d) potential of the plasma beam.

The time-resolved ion and electron currents are measured by applying a dc voltage of -50 V and 60 V, respectively, to the beam target (located at $z = 100$ mm) and measuring the voltage drop across a 10 Ω low-inductance resistor. When biased at -50 V, it is assumed that electrons are repelled from the beam target and hence only the ion current is collected. Alternatively, when the beam target is biased at 60 V both electrons and ions with energy greater than 60 eV, refer Figure 2 (a), are collected and hence the ion current can be subtracted from the total to yield the electron current. During the brief interval of sheath collapse, an increase in the electron current and decrease in the ion current is observed as shown in Figure 4 (b). As distinct from the ion current, which exhibits one clear modulation during each rf period, additional modulations are observed in the electron current within the decay envelope.

It is expected that the periodic modulations in optical emission shown in Figure 4 (c) are driven by the direct-impact excitation of the Ar($2p_1$) energy level. Here, it is important to note that the temporal position of the spatially averaged optical emission has been adjusted in post-processing to align with the interval of sheath collapse at Grid 1. The observed modulations in the optical emission are consistent with the measurements of electron current shown in Figure 4 (b), although the decay time for the optical emission is larger. While it is reasonable to suggest that the higher-frequency modulations observed in the electron current could potentially be mirrored in the excitation rate, it is not possible to extract this information due to the limited temporal resolution of the current experimental setup. The relatively weak modulation of the temporally resolved optical emission is consistent with the elongation of the effective lifetime due to cascade processes populating the Ar($2p_5$) level, as discussed earlier.

The temporal variation of lower-energy species, e.g. in the background plasma downstream of the source exit, is included in the measurements of time-resolved ion current, electron current and beam potential. It is therefore reasonable to suggest that their response to the propagation of relatively energetic ions and electrons during the sheath collapse at Grid 1 can be responsible for the additional modulations observed, e.g. electron current Figure 4 (b), after the Grid 1 sheath re-forms. Further work to limit the influence of experimental boundary conditions, including the pumping rate and location of the propagation chamber wall, is ongoing to understand these mechanisms in greater detail.

As shown in Figure 4 (d), the time-resolved potential of the floating beam target ϕ

is observed to rapidly decrease from 16 V to 1 V at the same time as the grid voltage approaches 0 V and the sheath at Grid 1 collapses. This is closely correlated with the onset of modulations in the electron current (increase), ion current (decrease) and spatially averaged optical emission (increase). Each minima in the beam potential corresponds to a brief interval when the sheath at Grid 1 collapses and electrons propagate from the source. Subsequently, for $V > 0$ V the sheath re-forms, effectively stopping the flux of these electrons and increasing the beam potential due to the relative increase in positive ion flux.

In conclusion, phase-resolved optical emission spectroscopy has been applied in combination with electrical measurements (ion and electron energy distribution functions, ion and electron currents and beam potential) to study the transient propagation of energetic electrons in a flowing plasma generated by an rf self-bias driven plasma thruster. The results suggest that the propagation of electrons during the interval of sheath collapse at the extraction grids acts to compensate space-charge in the plasma beam.

The authors wish to thank T. Lafleur and T. Gans for useful discussions and the York-Paris CIRC for financial assistance. This work has been done within the LABEX Plas@Par project, and received financial state aid managed by the "Agence Nationale de la Recherche", as part of the "Programme d'Investissements d'Avenir" under the reference ANR-11-IDEX-0004-02. It was also supported by a Marie Curie International Incoming Fellowship within the 7$^{\text{th}}$ European Community Framework (NEPTUNE PIIF-GA-2012-326054).

[1] D. L. Meier, S. Koide, and Y. Uchida, Science **291**, 84 (2001).

[2] A. V. Ivlev, S. A. Khrapak, S. K. Zhdanov, G. E. Morfill, and G. Joyce, Phys. Rev. Lett. **92** (2004).

[3] A. Fruchtman, Phys. Rev. Lett. **96** (2006).

[4] P. H. Diamond, S.-I. Itoh, K. Itoh, and T. S. Hahm, Plasma Phys. Control. Fusion **47**, R35 (2005).

[5] K. Ida and J. E. Rice, Nucl. Fusion **54**, 045001 (2014).

[6] C. Charles and R. Boswell, Appl. Phys. Lett. **82**, 1356 (2003).

[7] L. Garrigues and P. Coche, Plasma Phys. Control. Fusion **53**, 124011 (2011).

[8] S. Mazouffre, Plasma Sources Sci. Technol. **25**, 033002 (2016).

[9] D. M. Goebel and I. Katz, *Fundamentals of Electric Propulsion* (Hoboken, USA: Wiley, 2008).

[10] C. Charles, J. Phys. D: Appl. Phys. **42**, 163001 (2009).

[11] D. Rafalskyi and A. Aanesland, Plasma Sources Sci. Technol. **25**, 043001 (2016).

[12] D. Rafalskyi and A. Aanesland, J. Phys. D: Appl. Phys. **47**, 495203 (2014).

[13] D. Rafalskyi and A. Aanesland, Phys. Plasmas **22**, 063502 (2015).

[14] T. Lafleur, D. Rafalskyi, and A. Aanesland, Plasma Sources Sci. Technol. **24**, 015005 (2015).

[15] A. Greig, C. Charles, and R. W. Boswell, Front. Phys. **3** (2015).

[16] C. L. Ellison, Y. Raitses, and N. J. Fisch, Phys. Plasmas **19**, 013503 (2012).

[17] W. A. Hargus and M. A. Cappelli, Applied Physics B **72**, 961 (2001).

[18] J. Schulze, E. Schüngel, Z. Donkó, D. Luggenhölscher, and U. Czarnetzki, Journal of Physics D: Applied Physics **43**, 124016 (2010).

[19] T. Gans, D. O'Connell, V. Schulz-von der Gathen, and J. Waskoenig, Plasma Sources Science and Technology **19**, 034010 (2010).

[20] G. de Rosny, E. R. Mosburg Jr, J. R. Abelson, G. Devaud, and R. C. Kerns, Journal of Applied Physics **54**, 2272 (1983).

[21] F. Tochikubo, A. Suzuki, S. Kakuta, Y. Terazono, and T. Makabe, Journal of Applied Physics **68**, 5532 (1990).

[22] C. M. O. Mahony, R. Al Wazzan, and W. G. Graham, Applied physics letters **71**, 608 (1997).

[23] T. Gans, J. Schulze, D. O'Connell, U. Czarnetzki, R. Faulkner, A. R. Ellingboe, and M. M. Turner, Applied Physics Letters **89**, 261502 (2006).

[24] D. O'Connell, T. Gans, D. Vender, U. Czarnetzki, and R. Boswell, Physics of Plasmas **14**, 034505 (2007).

[25] K. Dittmann, D. Drozdov, B. Krames, and J. Meichsner, Journal of Physics D: Applied Physics **40**, 6593 (2007).

[26] D. W. Liu, F. Iza, and M. G. Kong, Applied Physics Letters **93**, 261503 (2008).

[27] V. Schulz-von der Gathen, L. Schaper, N. Knake, S. Reuter, K. Niemi, T. Gans, and J. Winter, Journal of Physics D: Applied Physics **41**, 194004 (2008).

[28] K. Niemi, S. Reuter, L. M. Graham, J. Waskoenig, N. Knake, V. Schulz-von der Gathen, and T. Gans, Journal of Physics D: Applied Physics **43**, 124006 (2010).

[29] J. E. Chilton, J. B. Boffard, R. S. Schappe, and C. C. Lin, Phys. Rev. A **57**, 267 (1998).

[30] M. A. Lieberman and A. J. Lichtenberg, *Principles of Plasma Discharges and Materials Pro-*

cessing, 2nd ed. (Wiley, New Jersey, 2005).

[31] J. Schulze, Z. Donkó, B. G. Heil, D. Luggenhölscher, T. Mussenbrock, R. P. Brinkmann, and U. Czarnetzki, Journal of Physics D: Applied Physics **41**, 105214 (2008).

[32] D. Rafalskyi and A. Aanesland, EPL (Europhysics Letters) **104**, 35004 (2013).